Laser pulse control of ultrafast heterogeneous electron transfer: A computational study

Luxia Wang and Volkhard May
Institut für Physik, Humboldt-Universität zu Berlin, Newtonstraße 15, D-12489 Berlin, Germany

Laser pulse control of the photoinduced 90 fs charge injection from perylene into the conduction band of TiO_2 is studied theoretically. The approach accounts for the electronic-ground state of the dye, the first excited state, the ionized state formed after charge injection, and the continuum of the electronic states in the conduction band, all defined vs a single reaction coordinate. To address different control tasks optimal control theory is combined with a full quantum dynamical description of the electron-vibrational motion accompanying the charge injection process. First it is proved in which way the charge injection time can be changed by tailored laser pulses. In a second step a pump-dump scheme from the perylene ground state to the first excited electronic state and back to the ground state is discussed. Because of the strong coupling of the excited perylene state to the band continuum of TiO_2 this control task is more suited to an experimental test than the direct control of the charge injection. © *2004 American Institute of Physics.* [DOI: 10.1063/1.1796274]

I. INTRODUCTION

To understand the details of heterogeneous electron transfer (HET) is of huge importance for different areas of research, for example, for the construction of Grätzel type solar cells.[1] These represent an attractive and low cost alternative to traditional silicon based photovoltaic devices. Grätzel cells are formed by dye sensitized nanocrystalline semiconductors, typically highly porous nanocrystalline anatase TiO_2. The rapid HET into an empty conduction band state of TiO_2 after photoexcitation of the dye is crucial (among other factors) for the light-harvesting efficiency. Once the electron is moved fast enough into TiO_2 surface states or into bulk conduction band states, any intramolecular side reactions can be suppressed. This fact initiated a number of ultrafast spectroscopic experiments (see, e.g., Refs. 2–9).

Since the S_1 level of *perylene* is degenerated with the conduction band of TiO_2, studies on this system have been favored. But interest moved also to ZnO or SnO_2. Moreover, different injection mechanisms have been compared including internal conversion processes or the formation of triplet states as well as charge motion through different conformations of the surface attached molecule. For the system alizarin on TiO_2 an injection time of 6 fs has been reported.[3]

In contrast to the intensive experimental studies of these processes less has been done to simulate the various steps of the charge injection process. A quantum chemical study on the absorption properties of anatase TiO_2 can be found in Ref. 10. Computations based on a classical description of the vibrational coordinates have been undertaken in Refs. 11 and 12. A wave packet propagation was used in Ref. 13 to compute frequency-domain spectra. References 14–16 discussed the full quantum dynamics of HET from perylene into TiO_2 as observed in Ref. 6. Although based on a minimal model for the electron-vibrational motion accompanying the charge injection this latter approach is capable to account for all main features of the reaction on a 100 fs time scale.

The present paper is devoted to an extension of our earlier studies on ultrafast HET given in Refs. 14–16. In the following we will focus on the case where a tailored laser pulse is used to initiate the charge injection process. The motivation for doing this is twofold. First, based on our simulations we would like to put forward a proposal for a proper experiment with the aim to influence the charge injection process. And second, it is of general interest to investigate laser pulse control where a state continuum is involved in the dynamics.

To carry out respective simulations we will use the model introduced in Refs. 14–16 (see also Fig. 1). It covers the electronic-ground state of the dye, the first excited state, the ionized state formed after charge injection, and the continuum of the electronic states in the conduction band. All molecular states are defined vs a single reaction coordinate. The continuum of TiO_2 conduction band states is accounted for by an expansion with respect to a complete orthogonal set of functions (see Refs. 15 and 16). Such a treatment is briefly recalled in Sec. II and in the Appendix. It is complementary to sophisticated electronic structure calculations (see, for example, Refs. 10 and 17) since it allows for a fully quantum dynamical description. To address the question of laser pulse control of heterogeneous electron transfer the optimal control theory (OCT) as described in, e.g., Refs. 18–23 is used (see Sec. III). The presentation of the numerical results in Sec. IV starts with the consideration of the charge transfer dynamics induced by a short Gaussian pulse. This will serve as a reference example. OCT is applied afterwards to study two control tasks in more details, one with the aim to populate the excited dye state as much as possible. In the other control task we undertake the attempt to hit a particular vibrational wave function in the electronic ground state. The paper ends with some concluding remarks in Sec. V.
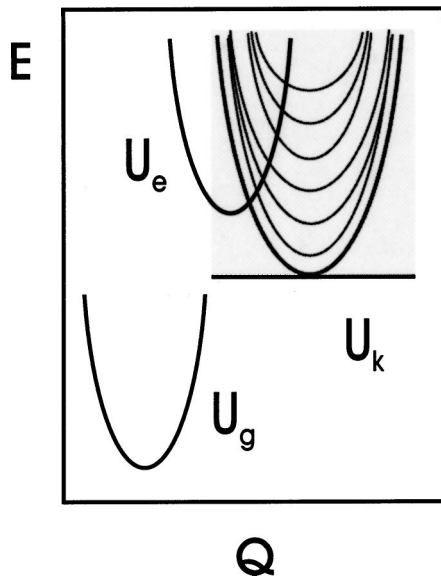
         8039

FIG. 1. Scheme of PESs vs a single reaction coordinate corresponding to the involved electronic levels in the used minimal model (the shaded area indicates the conduction band which covers a continuum of PES).

II. THE MODEL AND BASIC EQUATIONS OF MOTION

To describe laser pulse control of HET we start with a Hamiltonian adopted to the perylene-TiO$_2$ system. It reads

$$H(t) = H_{\text{mol-sem}} + H_{\text{field}}(t) \tag{1}$$

with the first part describing the molecule-semiconductor system. The second part is responsible for the coupling to the radiation field. For $H_{\text{mol-sem}}$ we use a three-level minimal model introduced earlier (cf. Refs. 14–16),

$$H_{\text{mol-sem}} = \sum_{a=g,e,\mathbf{k}} [E_a + H_a(q)] |\varphi_a\rangle\langle\varphi_a|$$

$$+ \sum_{\mathbf{k}} (V_{\mathbf{k}e} |\varphi_{\mathbf{k}}\rangle\langle\varphi_e| + \text{H.c.}). \tag{2}$$

It represents a certain diabatization with respect to the states of the surface adsorbed dye molecule coupled to the continuum of the conduction band states and includes the electronic ground state $|\varphi_g\rangle$, an excited electronic state $|\varphi_e\rangle$, and an ionized state formed after the electron transfer into the conduction band with states labeled by the wave vector $\mathbf{k}$. The concrete nature of the band states will be of less interest for the present studies. We only presume that they form a dense continuum. The coupling of the band states to the excited molecular state is given by $V_{\mathbf{k}e}$. The E_a introduced in $H_{\text{mol-sem}}$, Eq. (2) are electronic energies, where the band energy is written as $E_{\mathbf{k}} = E_c + \hbar\omega_{\mathbf{k}}$ with the lower band edge position E_c and with $\hbar\omega_{\mathbf{k}}$ characterizing the band width.

The vibrational Hamiltonians corresponding to the electronic states introduced so far are denoted by $H_a(q)$. The eigenfunctions and eigenvalues are given by χ_{aM} and $\hbar\omega_M$, respectively (M denotes the set of vibrational quantum numbers). We assume parabolic potential energy surfaces (PES) $U_a(q)$ for all electronic states with vibrational frequencies independent on the concrete state. The PES of the state with the electron in the conduction band corresponds to the ionized state of the molecule and will be denoted by U_{ion}. Al-

though the introduced model is more general, the concrete computations are restricted to the case of a single vibrational coordinate.

The coupling Hamiltonian to the radiation field is written in the standard dipole coupling form

$$H_{\text{field}}(t) = -\mathbf{E}(t)\hat{\mu}. \tag{3}$$

We assume that only an optical excitation from the molecular ground state to the excited molecular state is possible (as it is the case for perylene on TiO$_2$) and set

$$\hat{\mu} = \mathbf{d}_{\text{eg}} |\varphi_e\rangle\langle\varphi_g| + \text{H.c.} \tag{4}$$

The transition-dipole matrix element is denoted by $\mathbf{d}_{\text{eg}}$.

When studying the photoinduced dynamics on a 100 fs time scale it is reasonable to neglect any relaxational effect and to simply propagate the time-dependent Schrödinger equation related to the Hamiltonian introduced in Eq. (1). To solve the Schrödinger equation we carry out an expansion with respect to the diabatic electron-vibrational states $\chi_{aM}\varphi_a$ and obtain

$$|\Psi(t)\rangle = \sum_{aM} C_{aM}(t) |\chi_{aM}\rangle |\varphi_a\rangle. \tag{5}$$

Such a state expansion is fairly standard unless the presence of the band continuum leading to a continuous set $C_{\mathbf{k}M}(t)$ of expansion coefficients. We will tackle this problem as described in Refs. 15 and 16. Therefore, the $\mathbf{k}$ dependence of $C_{\mathbf{k}M}(t)$ is replaced by a frequency dependency, leading to the quantity $C_M(\omega;t)$, which, in a next step, will be expanded by the functions $u_r(\omega)$. They should form an orthogonal set which is complete along the energy range of the conduction band, here characterized by the frequency interval $[0,\omega_{\text{max}}]$ (from the lower to the upper conduction band edge). This allows us to write

$$C_M(\omega;t) = \sum_r u_r(\omega) C_M^{(r)}(t). \tag{6}$$

An appropriate truncation of the infinite sum leads to a finite set of expansion coefficients $C_M^{(r)}(t)$. The frequency dependence of the transfer coupling $V_e(\omega)$ (replacing V_{ke}) as well as that of the related density of states (DOS)

$$\mathcal{N}(\omega) = \sum_k \delta(\omega - \omega_{\mathbf{k}}) \tag{7}$$

will be specified later. As already demonstrated in Refs. 15 and 16 the expansion with respect to the functions $u_r(\omega)$ (substantiated by Legendre polynomials) reduces the effort to account for the continuous band energy enormously (compared to a naive discretization of the band energies). In the Appendix we present the complete set of equations of motion for the expansion coefficients and give some details on the used Legendre polynomials.

III. OPTIMAL CONTROL SCHEME

For the purposes here it suffices to use a scheme of laser pulse control of molecular dynamics where one asks to realize a certain state $|\Psi_{\text{tar}}\rangle$ (the target state) at time t_f (final time of laser pulse action) (Ref. 18). As it is well known the laser

pulse which solves this type of control task (the optimal pulse) can be derived from the extremum of the following functional (cf., e.g., Ref. 19)

$$J(t_f;\mathbf{E}) = |\langle \Psi_{\text{tar}}|\Psi(t_f)\rangle|^2 - \frac{1}{2}\int_{t_0}^{t_f} dt\, \lambda(t)\mathbf{E}^2(t). \quad (8)$$

This functional tries to realize a maximal overlap of the laser-pulse driven wave function $|\Psi(t)\rangle$ at time t_f with the target state under the constrain of a finite field strength of the pulse. In order to determine the extremum of $J(t_f;\mathbf{E})$ one fixes the penalty factor λ instead of the whole field-pulse intensity. Therefore, it is only possible to establish a relationship between the intensity and λ after the control problem has been solved. But Eq. (8) indicates that an increase of λ should result in a decrease of the pulse intensity. The time dependence of the Lagrangian multiplier $\lambda(t) = \lambda_0 \sin^{-2}(\pi t/t_f)$ has been introduced to realize a smooth switch on and switch off of the pulse at time t_0 and t_f, respectively.

The optimal pulse is obtained as the solution of the following functional equation (resulting from $\delta J = 0$)

$$\mathbf{E}(t) = -\frac{2}{\hbar\lambda(t)}\text{Im}\{\langle\Psi(t_f)|\Psi_{\text{tar}}\rangle\langle\Theta(t)|\hat{\mu}|\Psi(t)\rangle\}. \quad (9)$$

While $|\Psi(t)\rangle$ is obtained by the propagation of the Schrödinger equation starting with the initial value $|\Psi_0\rangle$, the state vector $|\Theta(t)\rangle$ follows from a backward propagation starting at t_f with the "initial" value $|\Psi_{\text{tar}}\rangle$. The notation of the functional equation for the optimal pulse via a forward and a backward wave function propagation allows to formulate an efficient iteration scheme.[20,21] One guesses an initial pulse to compute $|\Psi^{(0)}(t)\rangle$ from t_0 up to t_f. If one replaces the field strength $\mathbf{E}(t)$ of the pulse by Eq. (9) and therein $|\Psi(t_f)\rangle$ and $|\Psi(t)\rangle$ by the respective zero-order solution a first-order approximation $|\Theta^{(1)}(t)\rangle$ of the backward propagated state vector can be computed. Then, $|\Theta^{(1)}(t)\rangle$ is used to calculate $|\Psi^{(1)}(t)\rangle$ and so on. Within every iteration step an approximate optimal pulse $\mathbf{E}^{(n)}(t)$ follows from the iterated right-hand side of Eq. (9) (cf. Figs. 8 and 9).

Within the numerical calculations it is appropriate to use the Rabi energy $\hbar\Omega_{\text{Rabi}}(t) = \mathbf{d}_{\text{eg}}\mathbf{E}(t)$ instead of the field strength $\mathbf{E}(t)$ of the pulse. Then, by rewriting Eq. (9) λ_0 is replaced by $\Lambda_0 = 2|\mathbf{d}_{\text{eg}}|^2/\hbar^2\lambda_0$.

IV. NUMERICAL RESULTS

The results to be discussed hereafter are based on the reference model introduced in Sec. II with parameters adopted to the perylene-TiO$_2$ system (cf. Refs. 15 and 16). Therefore, the transition energy E_{eg} between the perylene ground state and the first excited state coupled to the TiO$_2$ conduction band continuum has been taken to be 2 eV. The same number has been chosen for the extension of the conduction band. The lower band edge E_c is positioned around 1 eV above the perylene ground state, but other cases are discussed, too.

Using the single vibrational coordinate model for perylene a vibrational energy $\hbar\omega_{\text{vib}}$ of 0.1 eV would be a good compromise for the different vibrational frequencies

observed for the molecule.[15] The reorganization energy λ_{ge} referring to the excitation of perylene amounts about 0.1 eV. In the single-coordinate approximation we have $\lambda_{ge} = \hbar\omega_{\text{vib}}g_{ge}^2$ with g_{ge} denoting the dimensionless electron vibration coupling constant. Accordingly this number is taken to be 1. However, the value of $\lambda_{e\,\text{ion}}$ characterizing the transition of an electron from the excited perylene state into the band continuum leaving behind an ionized molecule is not well known and will be varied around values of $g_{e\,\text{ion}} = 2$. To reproduce an injection time less than 100 fs observed in the experiment[6] the transfer coupling $V_{\mathbf{k}e} \equiv V_e(\omega)$ is taken about 0.1 eV. For the transition-dipole matrix element there does not exist a univocal value. We take 3 D, which is slightly higher than the value reported in Ref. 24. The present restriction to a minimal-model description, of course, represents a certain simplification. Therefore, it would be less useful to study effects of a frequency dependence of the transfer coupling and of the DOS, Eq. (7) (we use the constant values $\bar{V}_e$ and $\bar{\mathcal{N}}$, see below).

A. Reference dynamics

To obtain some reference results for the following discussion let us shortly inspect the transfer dynamics initiated by a Gaussian pulse of 30 fs duration full width at half maximum (FWHM) and a maximum field strength (at $t = t_{\text{pulse}}$) measured by the Rabi energy $\hbar\Omega_R = \mathbf{d}\mathbf{E}(t_{\text{pulse}}) = 0.1$ eV (we also set $E_c = 1$ eV and $\lambda_{ge} = \lambda_{e\,\text{ion}} = 0.1$ eV, for other parameters see below). Since the exciting field is given we only have to solve the time-dependent Schrödinger equation once, what is done via the state expansion, Eq. (5) with the initial condition $C_{aM} = \delta_{aM,g0}$ (referring to a zero-temperature situation).

Figure 2 displays the total population of the three involved electronic states

$$P_g(t) = \sum_M |C_{gM}(t)|^2, \quad (10)$$

$$P_e(t) = \sum_M |C_{eM}(t)|^2, \quad (11)$$

and

$$P_{\text{ion}}(t) = 1 - P_g(t) - P_e(t). \quad (12)$$

While the upper panel of Fig. 2 concentrates on a somewhat weaker case of transfer coupling ($\bar{V}_e = 0.02$ eV), a stronger coupling has been used in the lower panel of Fig. 2 ($\bar{V}_e = 0.1$ eV).

The chosen parameters of the weak coupling case result in a clear separation of the excited state population described by the increase of P_e, and the electron injection into the conduction band reflected by the subsequent decrease of P_e and the simultaneous increase of P_{ion}. In the strong coupling case there is no temporal separation of the charge injection process from the excited state population as demonstrated in the lower panel of Fig. 2. Now, the strong mixing of the excited molecular state with the band states results in a direct charge injection by the exciting pulse without intermediate excited state population. This behavior indicates that it
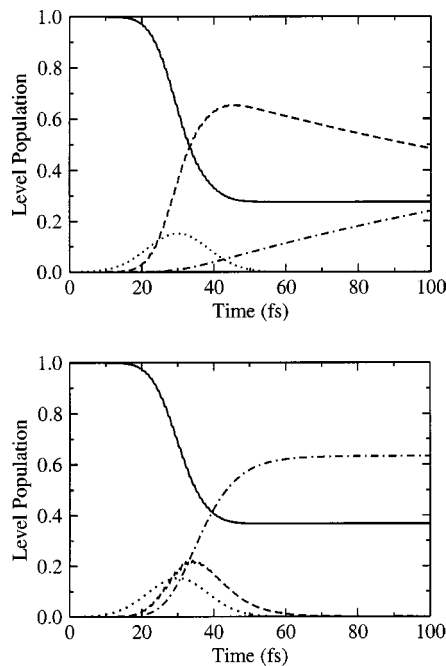
FIG. 2. Electronic level population after a 30 fs full width at half maximum (FWHM) laser pulse excitation in dependence on the transfer coupling $\bar{V}_e$ between the excited molecular state and the band continuum. Upper panel: $\bar{V}_e = 0.02$ eV, lower panel: $\bar{V}_e = 0.1$ eV, solid line: P_g, Eq. (10), dashed line: P_e, Eq. (11), dashed-dotted line: P_{ion}, Eq. (12), and dotted line: laser pulse envelope (in a.u.).

would be senseless in this case to speak about electron transfer (from the molecule into the semiconductor).

Next we discuss the probability distribution of the electron in the band continuum $P(\omega;t) = \Sigma_M |C_M(\omega;t)|^2$. It is shown in Fig. 3 for the situation presented in the lower panel of Fig. 2. Using the expansion, Eq. (6) the distribution is obtained as

$$P(\omega;t) = \sum_{r,p} u_r(\omega)u_p(\omega) \sum_M C_M^{(r)*}(t) C_M^{(p)}(t). \qquad (13)$$

The total electronic conduction band population [equivalent to P_{ion}, Eq. (12)] follows as $\int d\omega \mathcal{N}(\omega) P(\omega;t)$. Therefore, depending on the concrete form of the DOS $\mathcal{N}(\omega)$ the distribution $P(\omega;t)$ may become larger than 1 for particular values of ω.
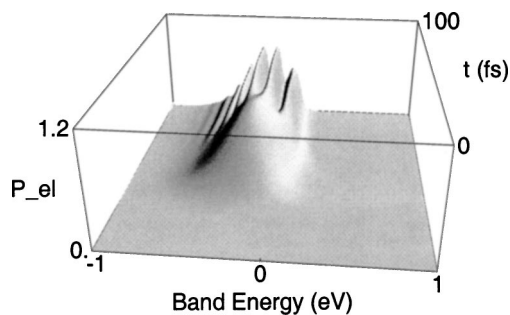

FIG. 3. Probability distribution of the injected electron, Eq. (13) vs the energy of the conduction band (parameters are identical with those taken to obtain the lower panel of Fig. 2, note that the band energy is arranged symmetrically around the injection position at $\hbar\omega = 0$).

It has already been indicated in Ref. 14 that $P(\omega;t)$ displays the vibrational progression of the involved reaction coordinate. Figure 3 demonstrates that after a certain time interval (reflecting energy-time uncertainty) the broad distribution decays into different peaks. Those correspond to transitions from the excited molecular state with energy $E_e + \hbar\omega_M$ into the band continuum with energy $E_c + \hbar\omega + \hbar\omega_N$. The possible energy values $\hbar\omega$ in the band follow as $E_e - E_c + \hbar(\omega_M - \omega_N)$ reflecting an inelastic charge injection accompanied by the creation or destruction of quanta of the vibrational coordinate. If the vibrational ground state of the excited molecular state would be populated only, $P(\omega;t)$ should extend to an energy range below $E_e - E_c$ (below 0 in Fig. 3). The simultaneous population of excited vibrational states may cause also structures in $P(\omega;t)$ above $E_e - E_c$. This would be the case after an ultrashort optical excitation, but is less obvious in Fig. 3.

To get convergent results a Legendre polynomial expansion up to the order 120 is required (for more details see the Appendix). The necessary number of vibrational levels depends somewhat on the used reorganization energies but never overcomes the value 22. Therefore, all studies discussed so far, in particular those resulting in Fig. 3 represent an important test for the polynomial expansion method. Its stability and convergency are essential for the different control scenarios discussed in the following sections. There, we first investigate in which manner the charge injection process can be influenced by a shaped laser pulse. In the second step, it will be discussed how the coupling to the band continuum disturbs the excitation deexcitation process of the first excited molecular state φ_e. Such an excitation scheme results in a time-dependent vibrational wave function in the electronic ground state, which should match at a certain time the target wave function (pump-dump scheme).

It would be also of interest to create a certain probability distribution $P_{\text{tar}}(\omega)$ in the band continuum. This, however, requires the introduction of a mixed target state $\int d\omega P_{\text{tar}}(\omega) |\varphi(\omega)\rangle\langle\varphi(\omega)|$ [note $\varphi(\omega) \equiv \varphi_{\mathbf{k}}$] or a superposition target state $|\Psi_{\text{tar}}\rangle = \int d\omega \sqrt{P_{\text{tar}}(\omega)} |\varphi(\omega)\rangle$. In order to concentrate the discussion in the present paper on the most obvious control scenarios we postpone investigations using such mentioned target states to a future study.

B. Laser pulse control of the excited state decay

In order to investigate the extent a shaped laser pulse modifies the charge injection process we consider a control task where one tries to completely populate a certain vibrational state at the excited electronic state φ_e at time t_f. The more involved formulation where the target state does not refer to a concrete vibrational state will be discussed later. Therefore, and in line with Sec. III we set $|\Psi_{\text{tar}}\rangle = |\chi_e^{(\text{tar})}\rangle |\varphi_e\rangle$, where $|\chi_e^{(\text{tar})}\rangle$ denotes a particular chosen vibrational target state specified below. Furthermore, we have to set up respective initial conditions to solve the time-dependent Schrödinger equations for forward and backward propagation by a state expansion like Eq. (5) (cf., e.g., Ref. 25). That for the forward propagation is identical with the initial condition given in the foregoing section and reads

TABLE I. Parameters used in Sec. IV B for studying laser pulse control of the excited state decay (case 1–4 are explained in the text; open positions refer to a variation of the respective parameter).

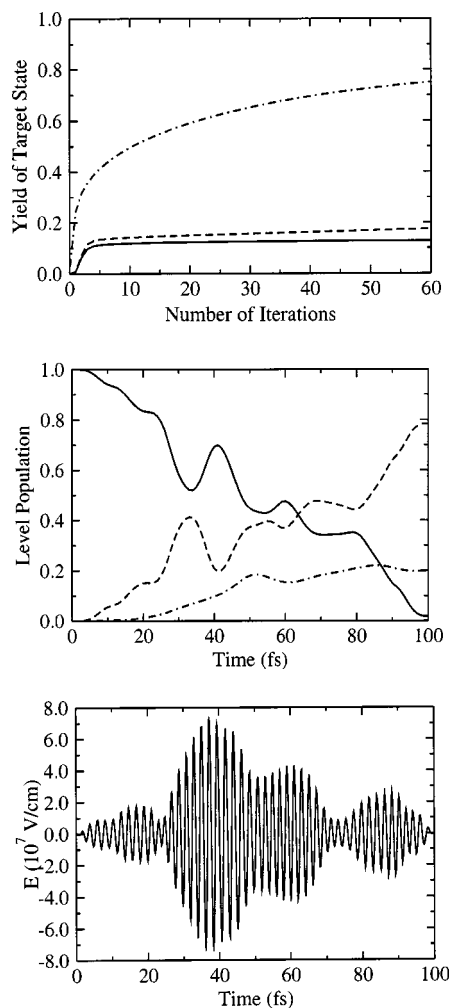|	E_c (eV)	$g_{e\,ion}$	g_{ge}	$\hbar\Lambda_0$ (eV)
1	$\cdots$	1.2	1.0	100
2	1	$\cdots$	1.0	100
3	1	2.2	$\cdots$	100
4	1	2.2	0.0	$\cdots$

FIG. 4. Laser pulse control of the excited state population of the surface attached molecule in dependence on the injection position E_c into the band continuum (for the concrete target state see text). Upper panel: control efficiency in dependence on the number of iteration steps (with $E_e = 2$ eV, solid curve: $E_c = 1$ eV, dashed curve: $E_c = 1.5$ eV, dashed-dotted curve: $E_c = 2$ eV). Middle panel: level populations P_g (solid curve), P_e (dashed curve), and P_{ion} (dashed-dotted curve) vs time for $E_c = 2$ eV (for all other parameters see text). Lower panel: temporal behavior of the optimal pulse for $E_c = 2$ eV.

$C_{aM} = \delta_{aM,g0}$ according to the zero-temperature case. If we denote the expansion coefficients of the state vector $|\Theta(t)\rangle$ (introduced in Sec. III and propagated backwards in time) by $B_{aM}(t)$ the initial condition for the backward propagation reads $B_{aM}(t_f) = \delta_{aM,eN_{tar}}$ with N_{tar} denoting the particular vibrational target state.

Within the computations discussed in the following a certain set of parameters has been fixed (see Sec. IV A): $E_e = 2$ eV, $\hbar\omega_{vib} = 0.1$ eV, $\bar{V}_e = 0.1$ eV, and $\bar{N} = 1$. The final time t_f amounts 100 fs. Since the taken value of $\bar{V}_e$ results in a charge injection time below 100 fs the solution of the control task requires a high field strength of the control pulse. Therefore, the penalty factor Λ_0 introduced in Sec. III has to be chosen large enough (cf. Table I).

The remaining parameters have been varied in the course of the computation and are given in Table I. The calculations labeled by 1 concentrate on the influence of the position of the lower conduction band edge E_c (relative to E_e). Respective results would be of interest when studying alternative dye sensitized semiconductors. The reorganization energy for the charge transfer from the excited molecular state into the conduction band continuum is varied in case 2 (variation via different coupling constants $g_{e\,ion}$) what is mainly motivated by reduced knowledge of the correct numbers for the perylene TiO$_2$ system. In case 3 we changed the reorganization energy for the transition from the ground state to the excited electronic state, again aimed to get an impression on the possible behavior of other systems. The reorganization energy is set equal to zero in the last case 4 where the field strength of the control pulse is altered via an alteration of Λ_0.

1. Change of the injection position into the band continuum

To study the influence of the injection position we take the vibrational ground state of the excited electronic state as the target state: $|\chi_e^{(tar)}\rangle = |\chi_{e0}\rangle$. The upper panel of Fig. 4 displays the target state population vs the number of iterations within the OCT scheme. If the excited molecular state is close to the bottom of the conduction band ($E_c = E_e$) the population of the target state achieves the value of 0.77. (Note the restriction to 60 iteration steps which might be enlarged a little bit here but would be sufficient for all other computations presented in this paper.) The population of the target state decreases considerably if E_c is lowered. Such a behavior is caused by a faster electron injection since E_e

enters a midband position. The decrease of the target state population goes along with a faster convergency of the iteration scheme.

The middle panel of Fig. 4 as well as Fig. 5 show the total populations P_g, P_e, and P_{ion}, Eqs. (10), (11), and (12), respectively, vs time (and after convergency within the iteration procedure has been obtained). While for the case $E_c = E_e$ the optimal pulse acts within the whole considered time interval (cf. the lower panel of Fig. 4), its action is restricted to the last 25 fs in the case of a midband position of E_e due to the faster electron injection. In both cases, however, a considerable depletion of the molecular ground state population has been achieved. Moreover, by comparing the population dynamics (middle panel of Fig. 4) with the temporal behavior of the optimal pulse (lower panel of Fig. 4) one may nicely realize how the optimal pulse solves the control task within the predetermined time interval of 100 fs by depopulation and partial repopulation of the ground state. The
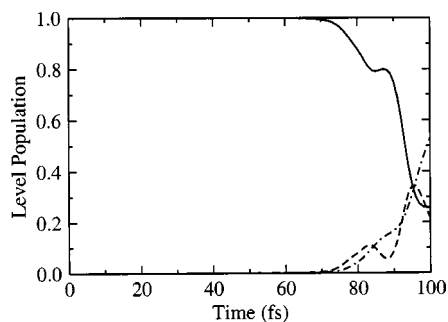
FIG. 5. Laser pulse control of the excited state population of the surface attached molecule for the injection position $E_c = 1$ eV into the band continuum (for the concrete target state see text). Shown are the level populations P_g (solid curve), P_e (dashed curve), and P_{ion} (dashed-dotted curve) vs time (for all other parameters see text).

FIG. 6. Electron distribution, Eq. (13) in the band continuum at time t_f. Solid curve: $E_c = 1$ eV, dashed curve: $E_c = 1.5$ eV, dashed-dotted curve: $E_c = 2$ eV (other parameters as in Fig. 4, note that the band energies are arranged symmetrically around the center at $\hbar\omega = 0$).

presence of population oscillations and thus the related separation of the optimal pulse by at least four overlapping subpulses may be reduced by reducing the target time t_f. However, such a case would be of less interest because choosing a smaller t_f would go along with a suppression of the influence of the band continuum. (Moreover, a systematic estimate how laser pulses obtained as a solution of the OCT may be realized in the experiment can be found in Ref. 26.)

To modify the control task discussed so far one may also ask about the maximization of the total population of state φ_e irrespective of a given distribution along the vibrational levels. This requires a modification of the control functional $J(t_f; \mathbf{E})$, Eq. (8) in replacing $|\langle \Psi_{tar} | \Psi(t_f) \rangle|^2$ by $\langle \Psi(t_f) | \times |\varphi_e\rangle\langle\varphi_e| \times |\Psi(t_f)\rangle$ (this notation becomes necessary since $\langle \chi_e | \Psi(t_f) \rangle$ remains a state vector in the vibrational state space). Then, one has to introduce $|\bar\Theta(t)\rangle = U(t, t_f)|\varphi_e\rangle\langle\varphi_e| \times |\Psi(t_f)\rangle$ which replaces $\langle \Psi_{tar} | \Psi(t_f) \rangle |\Theta(t)\rangle$ introduced in Eq. (9) [$U(t, t_f)$ denotes the total time-evolution operator corresponding to Hamiltonian $H(t)$, Eq. (1)]. The boundary conditions for the expansion coefficients $\bar B_{aM}(t)$ of $|\bar\Theta(t)\rangle$ read $\bar B_{aM}(t_f) = \delta_{a,e}C_{eM}(t_f)$, i.e., it is determined by the whole set of expansion coefficients for $|\Psi(t)\rangle$ at $t = t_f$. Carrying out similar computations as done for Fig. 5 the total population P_e of the target state at t_f becomes 0.39 in contrast to the much smaller value 0.21 of Fig. 5.

A detailed inspection of the middle panel of Fig. 4 indicates that a slight decrease of the band continuum population appears (between 50 and 60 fs and between 90 and 100 fs). This is related to the particular chosen configuration with the lower band edge being degenerated with E_e. If E_e has a midband position such recurrences from the continuum does not take place (cf. Fig. 5).

The energetic injection position also influences the distribution $P(\omega; t)$, Eq. (13) of the electron in the conduction band. This behavior of $P(\omega; t)$ is shown in Fig. 6 at the end of the control pulse $t = t_f$. As it has to be expected the localization of $P(\omega; t)$ depends on the position of E_e relative to the lower band edge E_c. However, also the shape of $P(\omega; t)$ strongly depends on this position. Since the discussed distribution is that defined via noneigenstates of the considered systems it completely vanishes if the lower band edge is reached.
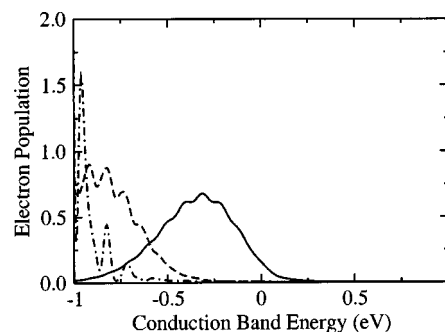
2. Change of the reorganization energies

As already mentioned the reorganization energy $\lambda_{e\,ion}$ for the excited-state band-continuum transition (excited-state cationic-state transition in the molecule) is not well known. Therefore, we will study the influence of $\lambda_{e\,ion}$ on the target state population (control yield) for the control task with a midband position of E_e as discussed in the Figs. 5 and 6. The following values for the yield have been obtained: 0.13, 0.17, and 0.25 for $\lambda_{e\,ion} = 0.1$, 0.48, and 0.68 eV ($g_{e\,ion} = 1, 2.2, 2.6$), respectively. With the increase of $\lambda_{e\,ion}$ (via an increase of $g_{e\,ion}$) the decay of the excited state is slowed down, which lets the control yield increase. And, at the same time, the increase of $\lambda_{e\,ion}$ leads to a decrease of P_{ion} (0.53, 0.48, and 0.42 for $g_{e\,ion} = 1$, 2.2, and 2.6, respectively). Such a behavior is caused by a less efficient electron injection due to a decreasing overlap between the PES of the excited and ionized molecular state. For the same reason, as shown in Fig. 7, $P(\omega; t)$ is distributed around a midband position if $g_{e\,ion}$ is small.

For this latter case ($g_{e\,ion} = 1$) Figs. 8 and 9 demonstrate the formation of the optimal pulse within a sequence of 60 iterations. Already the first three iteration steps change the pulse shape drastically. The drawn final shape (lower panel of Fig. 9) is nearly achieved after 30 iterations and undergoes only slight changes within the remaining iterations.
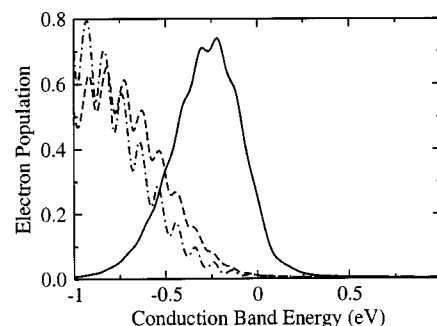

FIG. 7. Laser pulse control of the excited state population of the surface attached molecule. Shown is the electron distribution in the conduction band for different values of the reorganization energy $\lambda_{e\,ion}$ (solid line: $g_{e\,ion} = 1$, dashed line: $g_{e\,ion} = 2.2$, dashed-dotted line: $g_{e\,ion} = 2.6$, note that the band energies are arranged symmetrically around the center at $\hbar\omega = 0$).
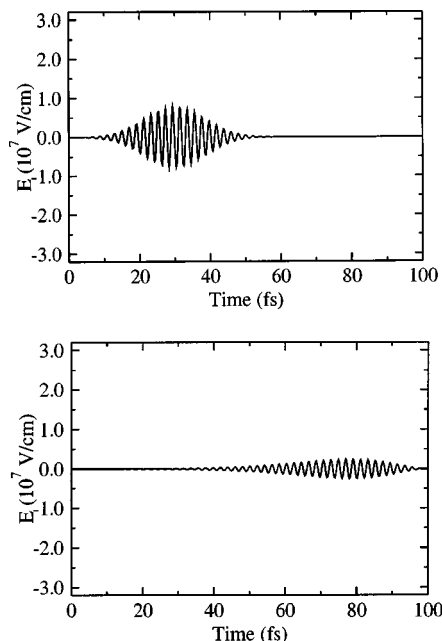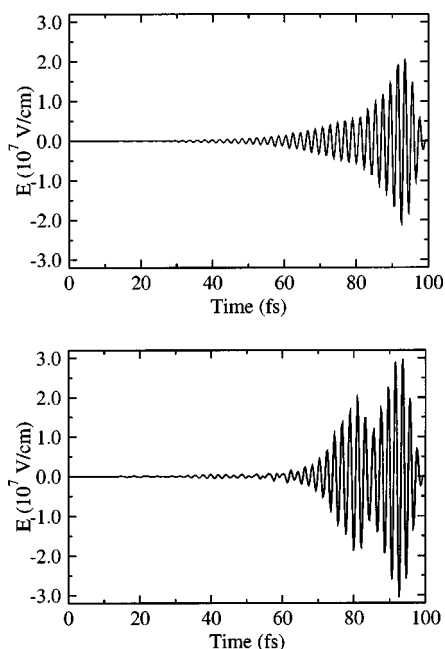
FIG. 8. Temporal behavior of different iterations $\mathbf{E}^{(n)}(t)$ of the optimal pulse referring to the control task explained in Fig. 7. Upper panel: initial guess, lower panel: first iterated form.
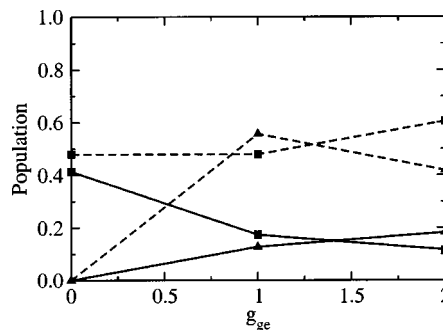

FIG. 10. Laser pulse control of the excited state population of the surface attached molecule. Shown are the target state population (full line) and the total band-continuum population (dashed line) vs the dimensionless coupling constant g_{ge} between the molecular ground state and the first excited electronic state (for other parameters see text). Curves with squares: vibrational ground state of the excited electronic state acts as the target state, curves with triangles: target state given by the second excited vibrational state.

change of λ_{ge} is achieved by changing the dimensionless coupling constant g_{ge} between 0 and 2 (for $E_c = 1$ eV and $g_{e\,\text{ion}} = 2.2$).

The results of the computation are displayed in Fig. 10 for a case where the vibrational ground state and the second excited vibrational level act as the target state ($t_f = 100$ fs). Shown are the population of the target state as well as of the band continuum (at t_f). With the increase of g_{ge} the control yield decreases by a considerable amount if the target state is given by the ground vibrational level. The behavior is reverse if we chose the second excited vibrational level as the target state. This goes along with a decrease of the total band-continuum population for $g_{ge} > 1$.

As indicated in Sec. III an increase of λ_0 (decrease of $\Lambda_0 = 2|\mathbf{d}_{eg}|^2/\hbar^2\lambda_0$) leads to a decrease of the field-pulse intensity. Increasing $\hbar\Lambda_0$ from 5 to 25, 50, and 100 eV our computations give an increase of the control yield as 0.06, 0.26, 0.34, and 0.41, respectively (for the same control task as in the foregoing section where the vibrational ground state of the excited electronic level defined the target state). The results show that increasing Λ_0 by a factor of 10 increases the target state population from 0.06 to 0.41.

C. Laser pulse control of the vibrational motion in the electronic ground state

In order to circumvent the destructive influence of the conduction band continuum on the solution of the control tasks described in the preceding section we will next consider the case where the target state is located in the electronic ground state (cf., e.g., Ref. 27). We set $\Psi_{\text{tar}} = \chi_{\text{tar}}\varphi_g$ with χ_{tar} given by the vibrational ground state wave function but shifted away from the minimum of the respective PES (away from $q = 0$). The shift will be characterized by the dimensionless quantity g_{shift} already introduced to fix the relative position of the different PES. The parameters which kept fix in the calculations are $E_e = 2$ eV, $\hbar\omega_{\text{vib}} = 0.1$ eV, $g_{ge} = 1$, $\bar{N} = 1$, $\hbar\Lambda_0 = 5$ eV, and $t_f = 100$ fs. In similarity to the foregoing section, other parameters are varied (cf. Table II).

In continuing the discussion of the preceding part we next concentrate on the effect originated by a change of the reorganization energy λ_{ge} governing the transition from the molecular electronic ground state into the excited state. Such a change results in a different preparation process of a wave packet in the state φ_e and we might expect an influence on the control yield (if λ_{ge} is small, the population of low-lying vibrational levels in the excited state can be increased). The

FIG. 9. Temporal behavior of different iterations $\mathbf{E}^{(n)}(t)$ of the optimal pulse referring to the control task explained in Fig. 7. Upper panel: third iterated form, lower panel: final form of the pulse (after 60 iterations).

TABLE II. Parameters used in Sec. IV C for the study of the laser pulse control of the vibrational motion in the electronic ground state (indicated are example 1 to 4 explained in the text, open positions refer to a variation of the respective parameter).

	E_c (eV)	$g_{e\,ion}$	$\bar{V}_e$ (eV)	g_{shift}
1	$\cdots$	1.5	0.1	0.5
2	1	$\cdots$	0.1	0.5
3	1	1.5	$\cdots$	0.5
4	1	1.5	0.1	$\cdots$

Noting Fig. 11 the same effect becomes obvious as already discussed in Sec. IV B. If the excited electronic level E_e is near the lower edge of the conduction band the control yield is larger than for E_e in a midband position. However, the present control task results in a much higher yield than the related one of the foregoing section. The high control yield of the case $E_e = E_c$ is related to a very small residual population of the band continuum (middle panel of Fig. 11)
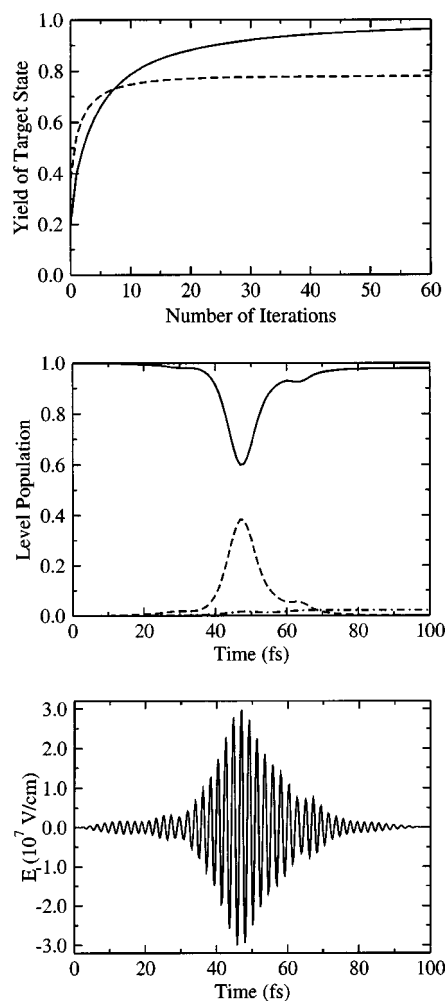

FIG. 11. Laser pulse control of the vibrational motion in the electronic ground state. Variation of the injection position E_c into the band continuum. Upper panel: control efficiency vs the number of iteration steps, solid line: $E_c = 2$ eV, dashed line: $E_c = 1$ eV. Middle panel: Level population P_g (solid line), P_e (dashed line), and P_{ion} (dashed-dotted line) vs time for $E_c = 2$ eV (for other parameters see text). Lower panel: temporal behavior of the optimal pulse for $E_c = 2$ eV.
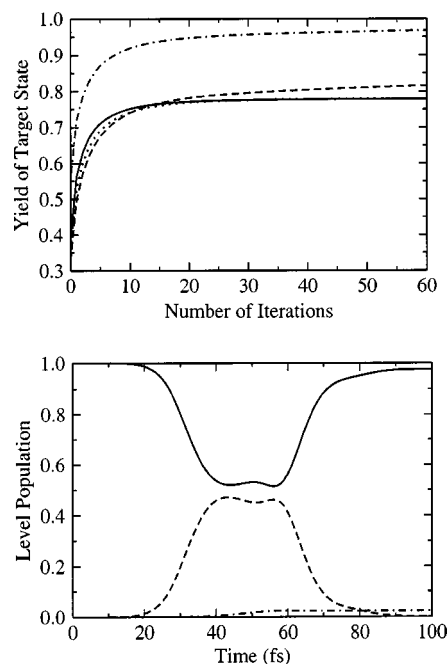

FIG. 12. Laser pulse control of the vibrational motion in the electronic ground state. Variation of the reorganization energy. Upper panel: yield of the target state in dependence on the number of iteration steps. Solid line: $g_{e\,ion} = 0.5$, dotted line: $g_{e\,ion} = 2$, dashed line: $g_{e\,ion} = 2.5$, dashed-dotted line $g_{e\,ion} = 5$. Lower panel: Level population P_g (solid line), P_e (dashed line), and P_{ion} (dashed-dotted line) vs time for $g_{e\,ion} = 5$ (other parameters see text).

indicating again the particular property of this energy level configuration. It is interesting to note that the intermediate population of the excited electronic level in the molecule is centered around 50 fs although $t_f = 100$ fs. In line with this observation the related optimal pulse shown in the lower panel of Fig. 11 covers about one third of the whole time interval. Its shape, however, differs strongly from a simple Gaussian one.

1. Change of the reorganization energy for the transition from the excited state into the band continuum

The reorganization energy $\lambda_{e\,ion}$ can be changed by a variation of $g_{e\,ion}$. As mentioned in Sec. IV B an increase of $g_{e\,ion}$ may slow down the electron injection from the excited state into the conduction band and, in this manner, may increase the target yield. But with the parameters chosen in this section this phenomenon is not observable for $g_{e\,ion} < 2.0$ as demonstrated in the upper panel of Fig. 12. The target yield almost keeps the same value up to an increase of $g_{e\,ion}$ beyond 2. For the smaller values of the reorganization energy (corresponding to $g_{e\,ion} < 2.0$) the tendency of the excited electron to move into the conduction band continuum is suppressed by the control field in a way resulting in a control yield less than 78%. For $g_{e\,ion} > 2.5$, as shown in the lower panel Fig. 12 the electron transfer from the excited state into the band continuum is strongly suppressed and the control yield amounts 96% (for $g_{e\,ion} = 5$).
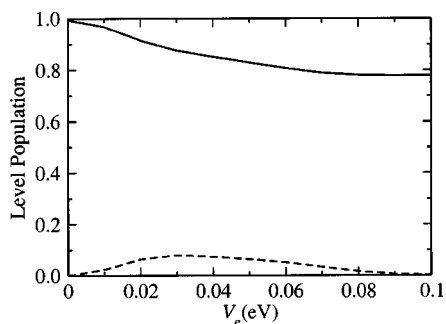
FIG. 13. Laser pulse control of the vibrational motion in the electronic ground state. Variation of the coupling strength $\bar{V}_e$ between the excited state and the ionized state. Shown are the population of the target state (solid line) and of the ionized state (dashed line) vs the coupling strength $\bar{V}_e$.

2. Change of the transfer coupling between the excited molecular state and the band continuum

Increasing $\bar{V}_e$ one has to expect a decrease of the injection time into the conduction band continuum. For the present control task, however, the effect of an increase of $\bar{V}_e$ is less direct. From Fig. 13 it is found that the increase of $\bar{V}_e$ only leads to a moderate decrease of the target state population reaching a constant value when $\bar{V}_e$ is beyond 0.08 eV. At the same time the population of the conduction band decreases and becomes very small (this population moves through its maximum for $\bar{V}_e$ about 0.03 eV). Since the decay into the continuum is accelerated with an increase of $\bar{V}_e$ the optimal pulse has to act again this tendency.

The displacement of χ_{tar} from $q=0$ (increase g_{shift}) lets decrease the control yield remarkably. The concrete values for $g_{shift}=0.5$, 1.0, 1.5, and 2.0 are 0.78, 0.39, 0.19, and 0.06, respectively. The related increase of the conduction band population shows a saturation at 0.42 for $g_{shift}>1.5$. This saturation is caused by the temporal behavior of the level populations as shown in Fig. 14, which also becomes independent on the position of the target state.

V. CONCLUSIONS

Femtosecond laser pulse control has been discussed for the particular case of heterogeneous electron transfer from perylene adsorbed at TiO_2 into the conduction band of the semiconductor. To describe the photoinduced 90 fs charge injection process a reference model has been introduced comprising the electronic-ground state of the dye, the first excited state, the ionized state formed after charge injection, and the continuum of the electronic states in the conduction band. To account for vibrational wave packet dynamics the molecular states are defined vs a single reaction coordinate. A fully quantum dynamical description of the electron-vibrational motion including the conduction band continuum of TiO_2 has been achieved by an expansion with respect to orthogonal polynomials.

Although parameters have been taken which resemble the system perylene on TiO_2 the present paper focuses on a more general clarification in which manner laser pulse control of heterogeneous electron transfer could be realized in the experiment. In order to do this two different control tasks
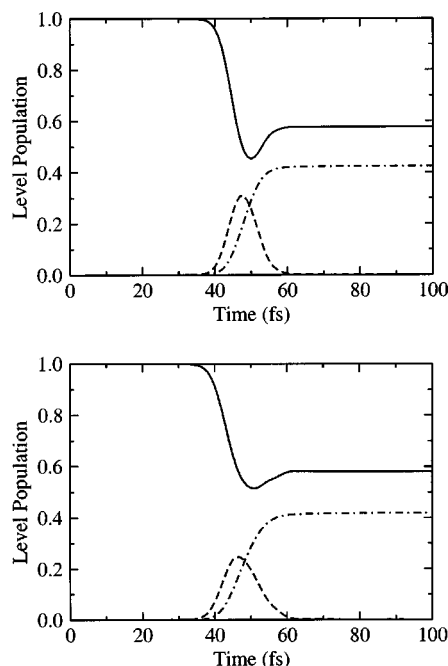

FIG. 14. Laser pulse control of the vibrational motion in the electronic ground state. Variation of g_{shift}. Shown are the level population P_g (solid line), P_e (dashed line), and P_{ion} (dashed-dotted line) vs time. Upper panel: $g_{shift}=1.5$, lower panel: $g_{shift}=2.0$.

have been investigated. In the first example one tries to control the excited state decay into the semiconductor band continuum. The other example uses a pump-dump-like scheme from the molecular ground state into the first excited electronic state (coupling to the band continuum), and then back into the ground state with a target state given by the displaced vibrational ground state. For the first case any control is strongly influenced by the coupling of the target state positioned in the first excited electronic state of the molecule to the band continuum. The control yield remains small (less than 20%) except the excited molecular level is near the lower band edge (a situation which does not correspond to the case of perylene on TiO_2).

In the second example where the band continuum influences a state, which is only populated during the motion to the target state the control yield becomes much larger (about 80% for a midband position of the excited molecular state typical for perylene on TiO_2). Such a control task seems to be much more appropriate for a study in the experiment. In particular, it represents a well-defined example for laser pulse guided dynamics where the wave packet moves from the initial state to the target state through intermediate states coupling to a continuum. In future work, of course, the used model needs different improvements, for example, the inclusion of additional levels bridging the excited molecular level and the band continuum. Related studies are just under work.

APPENDIX: POLYNOMIAL EXPANSION OF THE EQUATIONS OF MOTION

First, we present the set of coupled equations of motion for the expansion coefficients C_{aM} introduced in Eq. (5). These equations related to the conduction band continuum are rewritten using Eq. (6) where the continuum expansion coefficients $C_M^{(r)}(t)$ have been introduced ($\chi_{\text{ion } M}$ is the vibrational wave function of the ionized molecular state). The equations take the following form:

$$\frac{\partial}{\partial t} C_{gM}(t) = -i(E_g/\hbar + \omega_M) C_{gM}(t)$$
$$+ \frac{i}{\hbar} \mathbf{E}(t) \mathbf{d}_{ge} \sum_N \langle \chi_{gM} | \chi_{eN} \rangle C_{eN}(t), \quad (A1)$$

$$\frac{\partial}{\partial t} C_{eM}(t) = -i(E_e/\hbar + \omega_M) C_{eM}(t)$$
$$+ \frac{i}{\hbar} \mathbf{E}(t) \mathbf{d}_{eg} \sum_N \langle \chi_{eM} | \chi_{gN} \rangle C_{gN}(t)$$
$$- \frac{i}{\hbar} \sum_p \sum_N \langle \chi_{eM} | \chi_{\text{ion}N} \rangle \langle \mathcal{N} V_e u_p \rangle C_N^{(p)}(t),$$
$$(A2)$$

and

$$\frac{\partial}{\partial t} C_M^{(r)}(t) = -i(E_c/\hbar + \omega_M) C_M^{(r)}(t) - i \sum_p \langle \omega u_r u_p \rangle C_M^{(p)}(t)$$
$$- \frac{i}{\hbar} \sum_N \langle u_r V_e \rangle \langle \chi_{\text{ion}M} | \chi_{eN} \rangle C_{eN}(t). \quad (A3)$$

The bracket $\langle \cdots \rangle$ denotes frequency integration according to the relation

$$\langle u_r u_p \rangle \equiv \int_0^{\omega_{\max}} d\omega \, u_r(\omega) u_p(\omega) = \delta_{r,p}. \quad (A4)$$

The relation also indicates orthonormalization of the functions $u_r(\omega)$.

For the concrete calculations we used a particular realization of the orthonormal set u_r. It is given by the Legendre polynomials P_r according to the identification

$$u_r(\omega) = \sqrt{\frac{2r+1}{\omega_{\max}}} P_r[x(\omega)] \quad (A5)$$

with

$$x(\omega) = \frac{2\omega}{\omega_{\max}} - 1. \quad (A6)$$

The Legendre polynomials are defined by $P_0(x) = 1$, and for $r > 0$ by

$$P_r(x) = \frac{1}{2^r r!} \left(\frac{d}{dx} \right)^r (x^2 - 1)^r. \quad (A7)$$

Furthermore, they obey the relation

$$\int_{-1}^1 dx \, P_r(x) P_p(x) = \delta_{r,p} \frac{2}{2p+1}, \quad (A8)$$

from which the orthonormalization, Eq. (A4) of the functions u_r can be deduced. There exist the following recursion relation:

$$P_{r+1}(x) = \frac{2r+1}{r+1} x P_r(x) - \frac{r}{r+1} P_{r-1}(x), \quad (A9)$$

from which one obtains

$$\alpha_{r+1} u_{r+1}(\omega) = \left[\frac{2\omega}{\omega_{\max}} - 1 \right] u_r(\omega) - \alpha_r u_{r-1}(\omega) \quad (A10)$$

with

$$\alpha_r = \sqrt{\frac{r^2}{4r^2 - 1}}. \quad (A11)$$

Note $u_0(\omega) = 1/\sqrt{\omega_{\max}}$ and $u_1(\omega) = \sqrt{3/\omega_{\max}} \times (2\omega/\omega_{\max} - 1)$.

The use of the Legendre polynomials simplifies Eqs. (A3). We note

$$\langle \omega u_r u_p \rangle \equiv \langle u_r \omega u_p \rangle$$
$$= \frac{\omega_{\max}}{2} \langle u_r (\alpha_{p+1} u_{p+1} + u_p + \alpha_p u_{p-1}) \rangle$$
$$= \frac{\omega_{\max}}{2} (\delta_{r,p+1} \alpha_{p+1} + \delta_{r,p} + \alpha_p \delta_{r,p-1}). \quad (A12)$$

If we additionally provide a flat density of states $\bar{\mathcal{N}}$ and a frequency independent transfer coupling $\bar{V}_e$ it follows:

$$\langle u_r V_e \rangle = \delta_{r,0} \bar{V}_e \sqrt{\omega_{\max}} \quad (A13)$$

and

$$\langle \mathcal{N} V_e u_p \rangle = \delta_{p,0} \bar{\mathcal{N}} \bar{V}_e \sqrt{\omega_{\max}}. \quad (A14)$$

For all numerical calculations explained in the present paper we used these two latter approximations which further simplify the basic equations of motion (A1)–(A3). The necessary number of the polynomials did not exceed 120 whereas the upper vibrational number was $M = 22$.

[1] M. Grätzel, Nature (London) **414**, 338 (2001).
[2] Y. Tachibana, S. A. Haque, I. A. Mercer, J. E. Moser, D. R. Klug, and J. R. Durrant, J. Phys. Chem. B **105**, 7424 (2001).
[3] R. Huber, J. E. Moser, M. Grätzel, and J. Wachtveitl, J. Phys. Chem. B **106**, 6494 (2002).
[4] R. Huber, J. E. Moser, M. Grätzel, and J. Wachtveitl, Chem. Phys. Lett. **285**, 39 (2002).
[5] S. Pelet, M. Grätzel, and J. E. Moser, J. Phys. Chem. B **107**, 3215 (2002).
[6] C. Zimmermann, F. Willig, S. Ramakrishna, B. Burfeindt, B. Pettinger, R. Eichberger, and W. Storck, J. Phys. Chem. B **105**, 9245 (2001).
[7] J. Pan, G. Benkö, Y. H. Xu, T. Pascher, L. C. Sun, V. Sundström, and T. Polivka, J. Am. Chem. Soc. **124**, 13949 (2002).
[8] G. Benkö, B. Skarman, R. Wallenberg, A. Hagfeldt, V. Sundström, and A. P. Yartsev, J. Phys. Chem. B **107**, 1370 (2003).
[9] G. Benkö, P. Myllyperkiö, J. Pan, A. P. Yartsev, V. Sundström, J. Am. Chem. Soc. **125**, 1118 (2003).
[10] P. Persson, R. Bergström, and S. Lunell, J. Phys. Chem. B **104**, 10348 (2000).
[11] W. Schmickler and J. Mohr, J. Chem. Phys. **117**, 2867 (2003).
[12] W. Stier and O. V. Prezhdo, J. Phys. Chem. B **106**, 8047 (2002).
[13] L. C. T. Shoute and G. R. Loppnow, J. Chem. Phys. **117**, 842 (2002).
[14] S. Ramakrishna, F. Willig, and V. May, Phys. Rev. B **62**, R16330 (2000).

[15] S. Ramakrishna, F. Willig, and V. May, Chem. Phys. Lett. **351**, 242 (2002).

[16] S. Ramakrishna, F. Willig, V. May, and A. Knorr, J. Phys. Chem. B **107**, 607 (2003).

[17] W. Stier and O. V. Prezhdo, J. Phys. Chem. B **106**, 8047 (2002).

[18] A. P. Pierce, M. A. Dahleh, and H. Rabitz, Phys. Rev. A **37**, 4950 (1988).

[19] Y. J. Yan, R. E. Gillian, R. M. Whitnell, K. R. Wilson, and S. Mukamel, J. Phys. Chem. **97**, 2320 (1993).

[20] W. Zhu, J. Botina, and H. Rabitz, J. Chem. Phys. **108**, 1953 (1998).

[21] W. Zhu and H. Rabitz, J. Chem. Phys. **109**, 385 (1998).

[22] P. Kral, Z. Amitay, and M. Shapiro, Phys. Rev. Lett. **89**, 063002 (2002).

[23] V. May and O. Kühn, *Charge and Energy Transfer Dynamics in Molecular Systems* (Wiley-VCH, Berlin, 2004).

[24] T. M. Halasinski, J. L. Weisman, R. Ruiterkamp, T. J. Lee, F. Salama, and M. Head-Gordon, J. Phys. Chem. A **107**, 3660 (2003).

[25] S. Mukamel, *Principles of Nonlinear Optical Spectroscopy* (Oxford University, New York, 1995).

[26] T. Mancal and V. May, Chem. Phys. Lett. **362**, 407 (2002).

[27] J. A. Cina, D. S. Kilin, and S. Humble, J. Chem. Phys. **118**, 46 (2003).